Available online at www.sciencedirect.com
ScienceDirect
Infrared Physics & Technology 50 (2007) 211–216
INFRARED PHYSICS & TECHNOLOGY
www.elsevier.com/locate/infrared

Monolithically integrated near-infrared and mid-infrared detector array for spectral imaging

S.V. Bandara *, S.D. Gunapala, D.Z. Ting, J.K. Liu, C.J. Hill, J.M. Mumolo, S. Keo

Jet Propulsion Laboratory, California Institute of Technology, 4800 Oak Grove Drive, Pasadena, CA 91109, United States

Available online 16 January 2007

Abstract

A multi-band focal plane array sensitive in near-infrared (near-IR) and mid-wavelength infrared (MWIR) is been developed by monolithically integrating a near-infrared (1–1.5 μm) p–i–n photodiode with a mid-infrared (3–5 μm) QWIP. This multiband detector involves both intersubband and interband transitions in III–V semiconductor layer structures. Each detector stack absorbs photons within the specified wavelength band, while allowing the transmission of photons in other spectral bands, thus efficiently permitting multiband detection. Monolithically grown material characterization data and individual detector test results ensure the high quality of material suitable for near-infrared/QWIP dual-band focal plane array.

Keywords: Infrared imaging; Quantum well; Multicolor; Spectrometer

1. Introduction

The jet propulsion laboratory (JPL) is developing a snapshot hyperspectral imaging instrument that is capable of imaging a target in the 3–5 μm mid-wavelength infrared (MWIR) band and resolving several hyperspectral features within 1–1.5 μm near-infrared (NIR) band. The design of this instrument is based on a reflective computed-tomography imaging spectrometer (CTIS) with a monolithically integrated NIR and MWIR dual-band, 640×512 format focal plane array (FPA). The CTIS enables transient-event spectral imaging by capturing a scene's spatial and spectral information in every captured frame of the FPA. A CTIS records spatial and spectral information by imaging a scene through an optical relay system that has a two-dimensional (2D) grating disperser placed in collimated space [1–3]. This produces multiple, spectrally dispersed images of the scene that are recorded simultaneously in a single snapshot on the FPA. From the dispersed irradiance image and calibration information about the system, computed-tomography algorithms are used to reconstruct the spatial-spectral datacube representing the scene. Because CTIS systems utilize only fixed optics and do not require scanning of any type, they can be compact, rugged, and low cost.

This paper mainly focuses on the dual-band FPA design, fabrication, and performance of individual detectors. It includes a brief description of the reflective CTIS to understand the detector array requirements. A detailed description of the reflective CTIS can be found in the publications by our collaborators at JPL [1–3].

2. CTIS concept

The preliminary design of the reflective CTIS is shown in Fig. 1. A primary telescope (not shown) forms an image on the field stop of a reflective spectrometer. A 2D grating on the secondary convex mirror generates an array of spectrally dispersed images of the scene on the FPA. The zeroth order provides an undispersed gray-scale image of the scene in the center section of the FPA. The convex reflective grating of this CTIS was specifically designed to produce 3×3 diffraction orders with the following properties: (1) highly dispersed first orders with strong broadband efficiency in

* Corresponding author. Tel.: +1 818 354 7377; fax: +1 818 393 4540.
E-mail address: sumith.v.bandara@jpl.nasa.gov (S.V. Bandara).

1350-4495/$ - see front matter © 2006 Elsevier B.V. All rights reserved.
doi:10.1016/j.infrared.2006.10.030

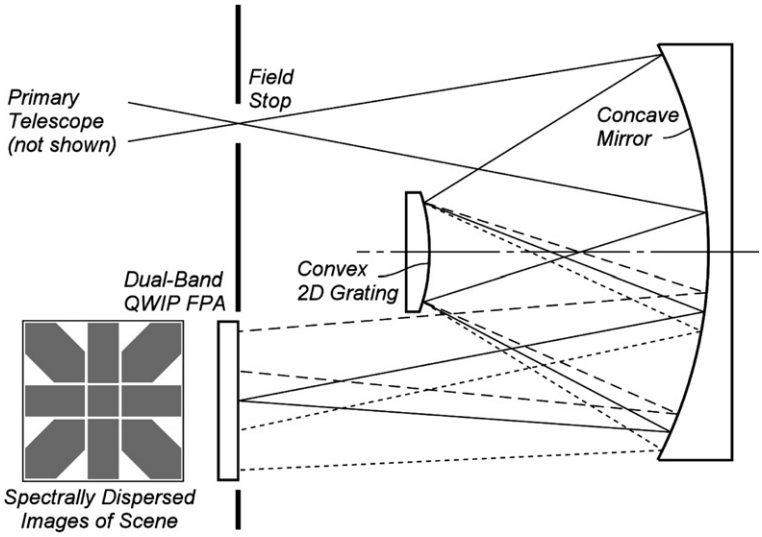

Fig. 1. The infrared CTIS and dual-band FPA. The CTIS produces an undispersed zeroth-order image with strong efficiency in the 3–5 μm band and highly-dispersed first-order images with strong broadband efficiency in the 1–1.5 μm band. The center section of the FPA is sensitive for 3–5 μm band, and surrounding sections are sensitive for the 1–1.5 μm band.

the 1–1.5 μm band and (2) an undispersed zeroth order with strong efficiency in the 3–5 μm band. The resulting grating design can be realized as a surface-relief profile fabricated by direct-write electron-beam lithography on a convex substrate. Following an initial system calibration, tomographic reconstruction algorithms are used in outer, higher-order images to determine the spectral characteristics of the scene in the 1–1.5 μm wavelength band. Spatial resolution is determined by the size of the zeroth order image on the FPA, which is naturally compressed by the surrounding dispersed orders. Thus, this CTIS requires a large-format, dual-band FPA that is capable of imaging in both MWIR (~3–5 μm) and NIR (~1–1.5 μm) spectral bands. Specifically, the center region of the array is sensitive in the 3–5 μm spectral band and the surrounding pixels of the array are sensitive in the 1–1.5 μm spectral band.

3. MID-IR/near-IR detector integration

The III–V materials-based QWIP technology is an excellent choice to develop the MWIR detector of the dual-band FPA because of its ability to integrate multi-quantum-well (MQW) stacks that are sensitive to different spectral bands. Each MQW stack absorbs photons within its specified wavelength band, thus permitting multiband detection. In addition, QWIP technology can provide highly uniform and stable FPAs (low $1/f$ noise) in larger formats, with pixel operability exceeding 99.9% [4–8]. Such unique properties of the FPA simplify on board data analysis, thus providing significant cost reduction in software development, data processing, and major system-level benefits upon integration. Furthermore, high yield in fabrication and reproducibility of this technology will result in a much lower cost for detector arrays than for competing technologies.

A typical QWIP consists of a 50-period MQW structure of quantum wells, separated by potential barriers, sandwiched between two contact layers [4,5]. Both contact layers and quantum-well layers are doped in order to provide carriers for photoexcitation. The QWIP detection mechanism involves photoexcitation of electrons between the ground and the first excited state subbands of quantum wells in the MQW structure (see Fig. 2) [4,5]. In order to optimize performance, MQW structure design places the first excited state exactly at the well top. This design feature is referred to a bound-to-quasibound quantum well [5]. The wavelength of the peak response and cutoff can be continuously tailored by varying well and barrier widths (layer thickness), barrier height (barrier composition), and carrier density (well-doping density) of the quantum wells. Commonly used GaAs substrate-based, $GaAs/Al_xGa_{1-x}As$ material system allows the quantum well parameters to be varied over a range wide enough to enable light detection at any wavelength range from 6 to 20 μm [4,10]. By adding a few monolayers of $In_yGa_{1-y}As$ during the GaAs quantum-well growth, the short wavelength limit can be extended to 3 μm [9]. In contrast, lattice matched InP/ $In_xGa_{1-x}As$/ In_yAl_{1-y}. As material-based quantum wells posses limited tailorability, because only a specific alloy composition, i.e., $x = 0.53$ and $y = 0.52$, could be grown nearly lattice-matched on InP substrates. This restricts the wavelength of the peak response to $\lambda_p \sim 4$ μm with $In_{0.53}Ga_{0.47}As/In_{0.52}Al_{0.48}As$ quantum wells, or to $\lambda_p \sim 7.5$ μm with $In_{0.53}Ga_{0.47}As/InP$ quantum wells [4,10]. However, these peak response wavelengths and spectral bandwidths can be altered to some extent by utilizing coupled quantum wells separated by thin barriers, while keeping the bound-to-quasibound design rule. Theoretically estimations show that the thickness of the thin barrier increases, responsivity spectrum

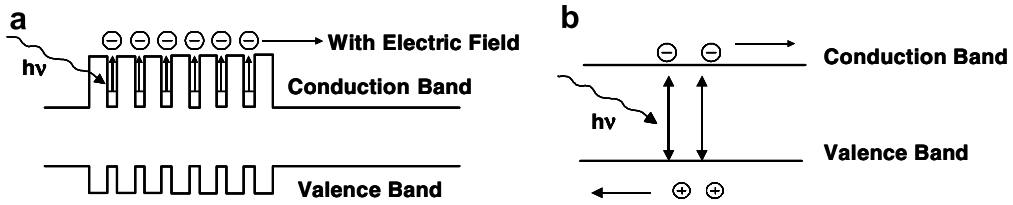

Fig. 2. (a) Schematic band diagram of a QWIP structure showing intersubband photoabsorption. (b) Schematic band diagram of an intrinsic semiconductor showing interband photoabsorption.

shifts towards the longer wavelengths. These QWIPs still operates under bound-to-quasibound conditions, which is achieved by adjusting the individual well width of the coupled wells. The spectral bandwidth of these QWIPs can be further increased by replacing single quantum wells with small superlattice structures (several quantum wells separated by thin barriers) in the multi-quantum-well structure [11]. Fig. 3 shows experimentally measured spectra of three different $In_{0.53}Ga_{0.47}As/In_{0.52}Al_{0.48}As$ QWIPs designed to respond at different wavelength bands.

Since the lower detection wavelength limit of an III–V-based QWIP is ~3 μm, the choice for the NIR detector of the FPA is obviously a semiconductor p–i–n photodiode utilizing interband transitions (see Fig. 2). Furthermore, our selection is limited to an InP substrate-based material system because the interband photoabsorption spectra of GaAs substrate-based p–i–n photodiodes cut off around ~1 μm. Thus, the active structure of the dual-band FPA includes $In_{0.52}Al_{0.48}As$ (barrier material)/$In_{0.53}Ga_{0.47}As$ (well material) MQW layers, and $In_{0.53}Ga_{0.47}As$ p–i–n photodiode monolithically grown on a lattice-matched InP substrate. NIR FPAs and imaging cameras using $In_{0.53}Ga_{0.47}As$ p–i–n photodiodes have been demonstrated and are currently available on the commercial market [12,13]. However, the JPL effort truly integrates a p–i–n photodiode utilizing interband transitions with a QWIP based on intersubband transitions to create an FPA capable of imaging in both the NIR and MWIR bands.

Fig. 4 shows a schematic of the layer structure of the monolithically grown wafer for the NIR/MWIR dual-band FPA. The structure consists of an $In_{0.53}Ga_{0.47}As/In_{0.52}Al_{0.48}As$-based MQW sandwiched between the heavily doped n-type $In_{0.53}Ga_{0.47}As$ contact layers and $InP(n^{++})/In_{0.53}Ga_{0.47}As$ (intrinsic)/InP (n-type) p–i–n photodiode layers. The QWIP stack is placed above the photodiode stack to avoid any NIR absorption by the QWIP layers, when the light incidents through the bottom surface. A thin $In_{0.52}Al_{0.48}As$ layer between the InP substrate and the active detector layers is used as a selective stop-etch layer during substrate thinning [5,6,8]. Typically, QWIP wafers are grown using molecular beam epitaxy (MBE), which provides sharp interfaces in multi-layer structures. However, the proposed NIR/MWIR dual-band FPA wafers are grown using metal organic Chemical vapor deposition (MOCVD) because it provides a high-purity material, i.e., with low background doping. Such intrinsically pure material layers are required to develop high-sensitive NIR p–i–n diodes. Fig. 5 shows the secondary ion mass spectroscopy (SIMS) data for the MOCVD-grown wafer. This figure clearly depicts the repeating $In_{0.52}Al_{0.48}As$ barriers in the QWIP region and the low-background impurity concentration in p–i–n diode region.

In order to characterize the MWIR QWIPs of the dual-band FPA wafer, large test mesas, from 200 μm to 400 μm in diameter, were fabricated using wet chemical etching and evaporation of Au/Ge ohmic contacts on the top and bottom contact layers [5–8]. The responsivity spectra of these

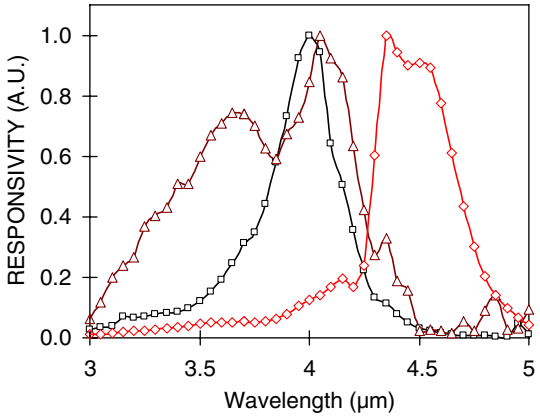

Fig. 3. Spectral tailoring of $In_{0.53}Ga_{0.47}As/In_{0.52}Al_{0.48}As$ QWIPs grown on lattice-matched InP substrate.

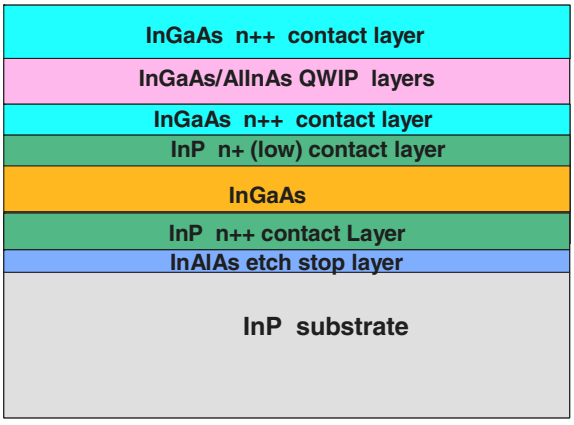

Fig. 4. Layer architecture of the MWIR QWIP and NIR p–i–n diode dual-color detector wafer.

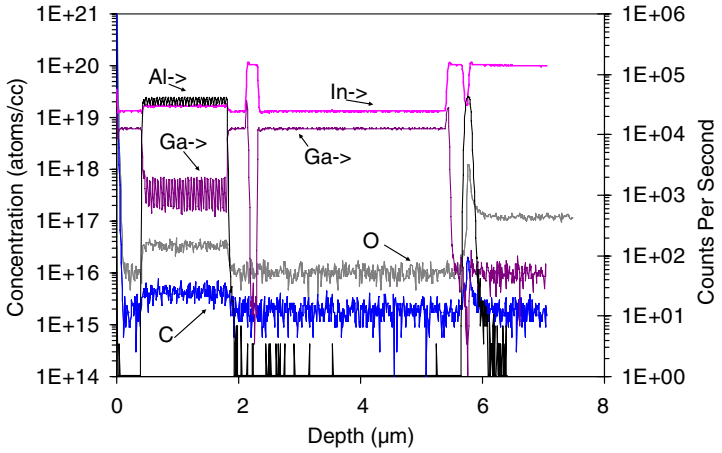

Fig. 5. Secondary ion mass spectroscopy (SIMS) data for the MOCVD-grown wafer. The periodic peaks of Al concentration show $In_{0.52}Al_{0.48}As$ barriers of 30-period QWIP. Impurity concentration plots also shows lower concentrations (carbon and oxygen) in the p–i–n diode layers.

detectors were measured using a 1000 K blackbody source and a grating monochromator. The detectors were back illuminated through a 45° polished facet to obtain normalized responsivity spectra at different bias voltages [5]. Then the absolute spectral responsivities were obtained by measuring the total photocurrent caused by a calibrated blackbody source. Fig. 6 shows the spectral responsivity curves measured at $T = 77$ K for $V_B = -1$ to -4 V bias voltage range. Spectral responsivity of an MOCVD-grown MWIR QWIP shows characteristics very similar to those of an MBE-grown MWIR QWIP, except for slight broadening in the MOCVD-grown detector response. This can be attributed to the thickness variation and nonsharp interfaces of the MOCVD-grown layers of the detector. Similarly, NIR detector material was characterized by fabricating 200×200 μm^2 test p–i–n diodes. These large-area diodes were fabricated by chemical etching and evaporating p- and n-type ohmic contacts on the top and bottom contact layers. The top metal contact was specifically designed to be a ring contact that allows illumination of the diode thorough the top layers. This scheme avoids unnecessary light absorption within the thick substrate material. Fig. 7 shows the spectral responsivity measured at different reverse bias voltages and operating temperatures. As expected, the long wave cutoff decreases as the temperature decreases due to the increase in the $In_{0.53}Ga_{0.47}As$ bandgap.

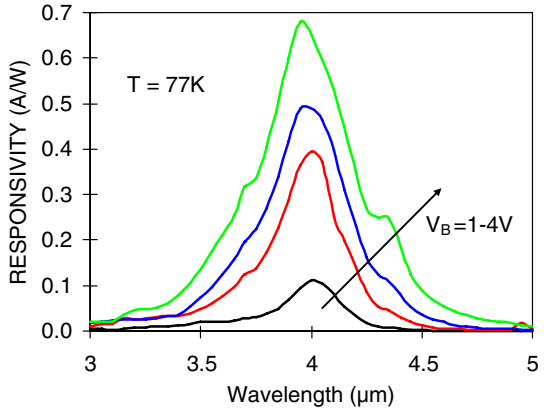

Fig. 6. Spectral sensitivity of $In_{0.52}Al_{0.48}As/In_{0.53}Ga_{0.47}As$ MWIR QWIP measured at different bias voltages and at temperature $T = 77$ K. The detector mesa is fabricated from a MOCVD-grown dual-band (MWIR QWIP and NIR p–i–n) wafer.

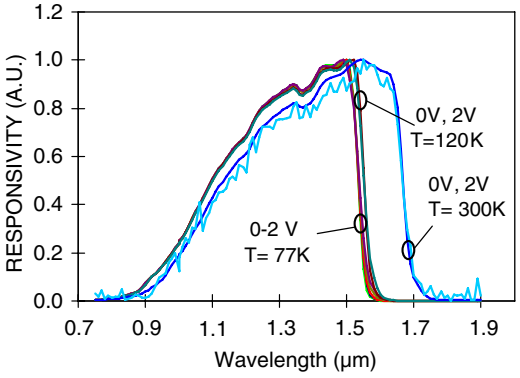

Fig. 7. Spectral responsivity of a $In_{0.53}Ga_{0.47}As$ NIR p–i–n diode measured at different reverse-bias voltages and temperatures.

4. MID-IR/near-IR focal plane array

Fig. 8 is a schematic diagram representing the dual-band detector array. As shown in the 3D representation, only MWIR QWIP pixels are activated in the central section of the dual-band array. Individual QWIP pixels are defined by photolithographic processing techniques and fabricated by wet and dry chemical etching through the photosensitive MQW layers into the n^{++} doped InP contact layer. Prior to this process, a light-coupling grating is fabricated on each QWIP pixel using lithographic and dry chemical processes [5,14,15]. Due to polarization-selection rules, QWIPs do not absorb light incident normal to the quantum well layers

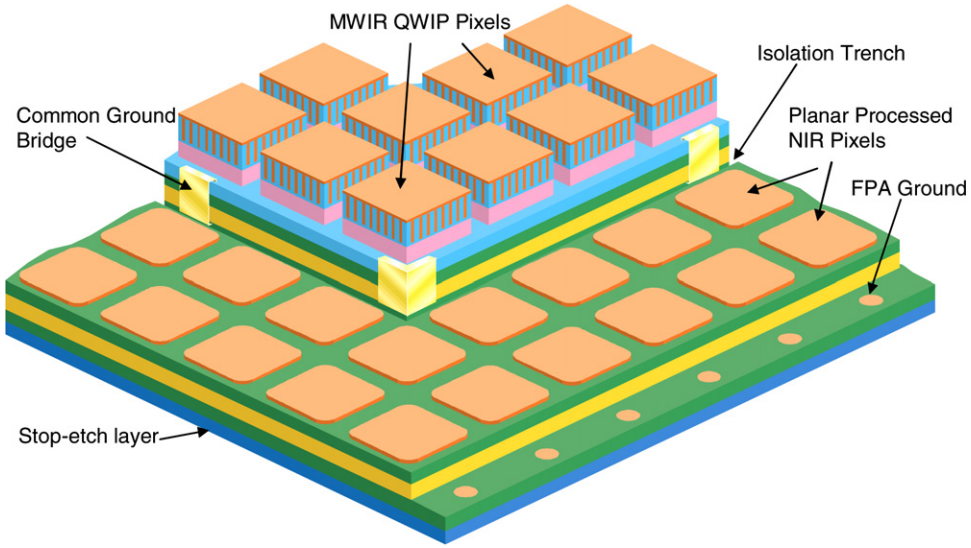

Fig. 8. Detector array architecture of the NIR/MWIR FPA (not to scale). MWIR QWIP pixels are isolated in the central area of the array. NIR p–i–n detector pixels are planar processed in the surrounding area of the array.

[4,5]. Thus, for imaging, it is necessary to fabricate a reflecting surface on top of the detector pixel to reflect light along the layer plane, enabling absorption [5,14,15]. The light coupling-gratings on top of the detector pixels will then be covered with Au/Ge and Au and it will serve as a contact to the active QWIP stack and function as a reflector. In order to isolate NIR pixels in the surrounding area of the array, all the QWIP layers are removed by chemical and dry etching. After defining pixels, using photolithography, p-type top contacts are created by diffusing impurities into the top n-type InP layer and evaporating metals on it. Fig. 8 also shows a trench around the periphery of the QWIP array to isolate the MWIR QWIP array area from the NIR p–i–n diode array. Metal strips running along the trench connecting the common bottom contact of the QWIP pixels to common bottom contact of the p–i–n diode pixels deactivate the unwanted p–i–n diode layers underneath the QWIP array. This also creates a common bottom contact for both QWIP and NIR pixels, which can be accessed from the exterior of the array. These contacts (n-type) are created by removing all the layers exterior to the array up to the bottom n^{++} InP layer. Once the dual-band detector array is fully developed, it will be hybridized to a commercially available CMOS readout multiplexer via Indium bump-bonding. As shown in Fig. 8, QWIP pixels have different heights than p–i–n diode pixels. The detector layer structure design was optimized to keep this height difference less than 2 μm across the detector array to ensure successful hybridization with the readout multiplexer via indium bump-bonding. The final hybrid will be thinned down to a membrane by removing the InP substrate and leaving the QWIP pixels and the bottom contact layer [5]. This thinned membrane will completely eliminate the thermal mismatch between the CMOS readout multiplexer and the InP-based QWIP/p–i–n FPA, and pixel-to-pixel optical cross-talk of the FPA.

Typically, $In_{0.53}Ga_{0.47}As$ p–i–n diode-based NIR FPAs operate at a very low reversed-bias voltage ($V_B \sim -100$ mV) at room temperature, $T \sim 300$ K, and the noise of these detectors is dominated by the Johnson noise. In contrast, MWIR QWIPs operate at a much lower temperature range, $T \sim 80$–120 K, and require up to $V_B \sim -2$ V reverse bias voltage. The dominant noise source of the QWIP is shot noise resulting from the total current through the detector. Since the read-out multiplexer could provide one fixed-bias voltage for every pixel in the array, the dual-band NIR/MWIR array will operate at $V_B \sim -2$V reverse bias and $T \sim 60$–160 K temperature range. These operating conditions are as precise as required by the QWIP detector, but deviate greatly from the NIR p–i–n diode operating parameters. However, increased-operating bias voltage of the p–i–n diode is counterbalanced by the lower operating temperature of the FPA. Fig. 9 clearly shows that the low

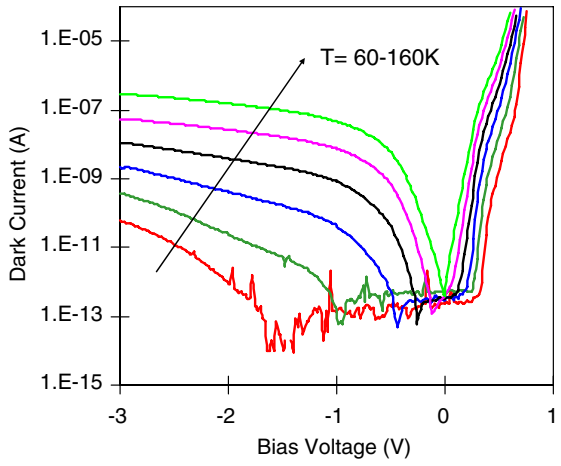

Fig. 9. Dark current of $In_{0.53}Ga_{0.47}As$ p–i–n diode at different operating temperatures. These currents are measured using 200 μm × 200 μm mesas and normalized to a 25 μm × 25 μm pixel size.

dark current at $V_B \sim -2$ V and $T \sim 60$–160 K, which is less than the typical dark currents at $V_B \sim -100$ mV and $T \sim 300$ K. Also, Fig. 8 shows no change in the responsivity spectrum of the p–i–n diode operating at higher-bias voltages. As operating temperature dropped, decrease in the long cutoff from $\lambda_C \sim 1.7$ μm to $\lambda_C \sim 1.55$ μm creates no dilemma because the responsivity spectrum still covers 1–1.5 μm the wavelength range required by the CTIS instrument.

5. Summary

In summary, a 640×512-format, NIR/MWIR dual-band FPA is being developed for a reflective computed-tomography imaging spectrometer. The detector array is fabricated from a monolithically grown $In_{0.53}Ga_{0.47}As/In_{0.52}Al_{0.48}As$ QWIP layer structure and an $In_{0.53}Ga_{0.47}As$ p–i–n diode layer structure on a lattice-matched InP substrate. Material characterization data and individual detector test results ensure the high quality of material suitable for NIR/QWIP dual-band focal plane array.

Acknowledgements

The authors gratefully acknowledge Daniel Wilson and William R. Johnson for many helpful discussions.

References

[1] D.W. Wilson, P.D. Maker, R.E. Muller, P.Z. Mouroulis, Computed tomography imaging spectrometer (CTIS) with 2D reflective grating for ultraviolet to long-wave infrared detection especially useful for surveying transient events, US Patent 6, 522, 403, Assigned to NASA, Feb. 18, 2003.

[2] W.R. Johnson, D.W. Wilson, G.H. Bearman, An all-reflective computed-tomography imaging spectrometer, in: Carl A. Nardell, Paul G. Lucey, Jeng-Hwa Yee, James B. Garvin (Eds.), Instruments, Science, and Methods for Geospace and Planetary Remote Sensing, Proceedings of the SPIE 5660, 2004, pp. 88–97.

[3] W.R. Johnson, D.W. Wilson, G.H. Bearman, All-reflective snapshot hyperspectral imager for UV and IR applications, Opt. Lett. 30 (2005) 1464–1466.

[4] B.F. Levine, J. Appl. Phys. 74 (1993) R1.

[5] S.D. Gunapala, S.V. Bandara, Quantum Well Infrared Photodetector (QWIP) Focal Plane Arrays, Semiconductors and Semimetals, vol. 62, Academic Press, 1999, pp. 197–282.

[6] S.V. Bandara, S.D. Gunapala, F.M. Reininger, J.K. Liu, S.B. Rafol, J.M. Mumolo, D.Z. Ting, R.W. Chuang, T.Q. Tring, J.M. Fastenau, A.W.K. Liu, SPIE 5074 (2003) 787.

[7] W. Cabanski, R. Breiter, R. Koch, K.H. Mauk, W. Rode, J. Ziegler, K. Eberhardt, R. Oelmaier, H. Schneider, M. Walther, Proc. SPIE 4028 (2000) 113.

[8] S.D. Gunapala, S.V. Bandara, J.K. Liu, C.J. Hill, S.B. Rafol, J.M. Mumolo, J.T. Trinh, M.Z. Tidrow, P.D. LeVan, Semicond. Sci. Technol. 20 (2005) 473–480.

[9] K.K. Choi, S.V. Bandara, S.D. Gunapala, W.K. Liu, J.M. Fastenau, J. Appl. Phys. 91 (2002) 5230.

[10] G. Hasnain, B.F. Levine, D.L. Sivco, A.Y. Cho, Appl. Phys. Lett. 56 (1990) 770.

[11] S.V. Bandara, S.D. Gunapala, J.K. Liu, E.M. Luong, J.M. Mumolo, W. Hong, D.K. Sengupta, M.J. McKelvey, Appl. Phys. Lett. 72 (1998) 2427.

[12] G.H. Olson, P.E. Dixon, M.J. Lange, J.J. Sudol, M.J. Cohen, A.R. Sugg, J.C. Dries, J. Cryst. Growth 222 (2001) 693–696.

[13] M.H. Ettenberg, M. O'Grady, S. Huang, M.J. Cohen, Proc. SPIE 5074 (2003) 353.

[14] J.Y. Andersson, L. Lundqvist, Z.F. Paska, J. Appl. Phys. 71 (1991) 3600.

[15] G. Sarusi, B.F. Levine, S.J. Pearton, S.V. Bandara, R.E. Leibenguth, J. Appl. Phys. 76 (1994) 4989.